FMCW SAR Sparse Imaging Based on Approximated Observation: An Overview on Current Technologies

Hui Bi, *Member, IEEE*, Daiyin Zhu, Guoan Bi, Bingchen Zhang, Wen Hong, *Senior Member, IEEE*, and Yirong Wu

***Abstract*—Sparsity-driven synthetic aperture radar (SAR) imaging technique for frequency modulation continuous wave (FMCW) has already shown the superiority in terms of performance improvement in imaging and recovery from down-sampled data. However, restricted by the computational cost, conventional FMCW SAR sparse imaging method based on observation matrix is not able to achieve the large-scale scene reconstruction, not to mention real-time processing. To solve this problem, the FMCW SAR sparse imaging theory based on approximated observation is proposed by using an echo simulation operator to replace typical observation matrix, and recovering the scene via 2-D regularization operation. This new technology can achieve high-resolution sparse imaging of the scene with a computational cost close to that of traditional matched filtering algorithms, which makes several applications, such as early-warning and battlefield monitoring, possible by using FMCW SAR sparse imaging system. In this article, we present the recent research progress on approximated observation-based FMCW SAR sparse imaging to deal with a few key issues for practical radar systems. In particular, we describe: first, L_q-norm $(0 < q \leq 1)$ regularization-based imaging technique that makes sparse reconstruction of large-scale scene possible; second, $L_{2,q}$-norm regularization-based imaging technique that minimizes the azimuth ambiguities in high-resolution sparse imaging; and third, a sparse imaging technique that supports real-time applications of FMCW SAR imaging.**

***Index Terms*—Approximated observation, frequency modulation continuous wave (FMCW), L_q-norm regularization, $L_{2,q}$-norm regularization, real-time imaging, sparse imaging, synthetic aperture radar (SAR).**

Manuscript received May 26, 2020; revised July 20, 2020 and August 9, 2020; accepted August 13, 2020. Date of publication August 18, 2020; date of current version August 31, 2020. This work was supported in part by the Fundamental Research Funds for the Central Universities under Grant NE2020004, in part by the National Natural Science Foundation of China under Grant 61901213, in part by the Natural Science Foundation of Jiangsu Province under Grant BK20190397, in part by the Aeronautical Science Foundation of China under Grant 201920052001, and in part by the Young Science and Technology Talent Support Project of Jiangsu Science and Technology Association. *(Corresponding author: Hui Bi.)*

Hui Bi and Daiyin Zhu are with the Key Laboratory of Radar Imaging and Microwave Photonics, Ministry of Education, Nanjing University of Aeronautics and Astronautics, Nanjing 211106, China, and also with the College of Electronic and Information Engineering, Nanjing University of Aeronautics and Astronautics, Nanjing 211106, China (e-mail: bihui@nuaa.edu.cn; zhudy@nuaa.edu.cn).

Guoan Bi is with the School of Electrical and Electronic Engineering, Nanyang Technological University, Singapore 639798, Singapore (e-mail: egbi@ntu.edu.sg).

Bingchen Zhang, Wen Hong, and Yirong Wu are with the Aerospace Information Research Institute, Chinese Academy of Sciences, Beijing 100094, China (e-mail: bczhang@mail.ie.ac.cn; whong@mail.ie.ac.cn; wyr@mail.ie.ac.cn).

Digital Object Identifier 10.1109/JSTARS.2020.3017487

I. Introduction

MODERN synthetic aperture radar (SAR) is an active microwave imaging system usually mounted on a flying platform to acquire high-resolution images of the ground by transmitting and receiving electromagnetic waves. Compared with optical imaging, SAR has an all-time and all-weather surveillance capability that has been widely used in military and civilian applications [1]–[3]. Compared with typical pulse mode, frequency modulation continuous-wave (FMCW) SAR has shown good potential in transmitted power and system cost reduction, and hence has been widely used for short-range imaging applications [4]–[6]. Up to now, several matched filtering (MF)-based algorithms, such as range-Doppler algorithm (RDA) [7], nonlinear frequency scaling algorithm (FSA) [8], wavenumber domain algorithm (WDA) [9], back-projection algorithm (BPA) [10], and chirp-Z algorithm [11] have been applied in FMCW SAR imaging to successfully obtain the well focused images of surveillance regions.

To satisfy the condition of Nyquist–Shannon sampling theory [12], [13], the amount of used data has to be increased for improving the imaging performance of SAR system [14]. Therefore, reducing the complexity of radar system becomes a critical issue of the system design and implementation for large-scale scene imaging. It is difficult, if not impossible, to use these MF-based methods to minimize the cost of radar system that produces high-resolution images from down-sampled data. In addition, high-resolution, wide-swath, and real-time processing have been currently the main requirements of modern SAR systems. This will significantly increase the amount of SAR data especially for the large-scale scene recovery. It is also become important to reduce system complexity and data volume [15]. To cope with these critical issues, sparse signal processing including compressive sensing (CS) technique [16]–[18] was introduced to SAR imaging to achieve high-resolution reconstruction of sparse scene [19]–[21]. In 2010, Patel *et al.* [22] developed an exact observation-based CS-SAR imaging model by discretizing the imaging geometry and transmitted signal exactly into an observation matrix, and used regularization technique to achieve the sparse recovery of considered scene. In 2012, Zhang *et al.* [23] demonstrated the concept and method of sparse SAR imaging. Then, Çetin *et al.* [24] summarized the typical observation matrix-based sparse SAR imaging theory and pointed out its application prospects in several fields. In 2013, Ender reported a brief review about CS-based radar imaging to express concerns that huge computational cost is required for

nonsparse scenes. Therefore, CS-SAR imaging may be problematic for practical SAR data processing [25]. According to these works of literature, conventional sparse SAR imaging method, i.e., observation matrix-based method [22]–[25], may need to address the following unsolved issues that are critical for any practical FMCW SAR radar systems.

1) *Large-scale scene sparse reconstruction*: Because 2-D raw data matrix has to be arranged into a vector to construct the observation matrix for every image point, the conventional FMCW SAR sparse imaging method generally requires inhibitive memory space for recovering large scale scenes. For a scene with 1024×8192 points, this method needs a memory space of 64 TB and more than 100 days of processing to achieve a focused image, which is nearly impossible and unacceptable to be supported by current computing facilities.
2) *Azimuth ambiguity suppression*: An important advantage of sparse SAR imaging is sparse scene recovery from down-sampled data achieved by reducing the system pulse repetition frequency (PRF) during data collection. This process will decrease the system complexity and improve the swath width simultaneously. It is known that the azimuth ambiguity, caused by the down-sampling operation, decreases the recovered image quality and increases the false alarming rate. Therefore, the issue of minimizing azimuth ambiguity should be studied for high-resolution FMCW SAR sparse imaging.
3) *Real-time imaging*: In military applications, such as battlefield warning and monitoring, real-time imaging is the key requirement of FMCW SAR system. However, since the computational complexity of observation matrix-based method is proportional to the square of scene size, the computation time is unbearable for large-scene recovery, not to mention real-time processing. This seriously restricts the application prospects of sparse imaging. Therefore, novel real-time FMCW SAR sparse imaging method has to be investigated to meet the real-time processing requirement.

In 2012, the approximated observation-based sparse imaging theory [23], [26], [27] was proposed, which uses an echo simulation operator to replace observation matrix, and recovers the scene of interest by 2-D regularization operation. In pulse-mode-based SAR imaging, this approximated observation-based method has been applied in Stripmap, Spotlight, Scan, TOPS SAR applications [26], [28]–[30], and successfully used in the airborne [31] and spaceborne [32] SAR data processing, which makes wide-swath high-resolution sparse imaging possible. To adequately deal with the above issues, in 2019, the idea of approximated observation was first introduced to FMCW SAR for practical sparse imaging [33]. Compared with MF-based methods, it improves the recovered image quality effectively in terms of suppressing sidelobes, noise, and clutter, and even obtains the high-resolution image from down-sampled echo data. Motivated by the concept of approximated observation, this article will present an overview on the theory of FMCW SAR sparse imaging to solve the abovementioned problems. The main contributions are summarized as follows.

1) Approximated observation-based FMCW SAR sparse imaging method is demonstrated with 2-D imaging model establishment, operator construction, azimuth-range decouple, and L_q-norm $(0 < q \leq 1)$ regularization recovery, which make sparse recovery of large-scale scene possible in FMCW SAR [23], [32], [33].
2) To suppress azimuth ambiguities, we construct a novel unambiguous FMCW SAR sparse imaging model, and propose an approximated observation-based $L_{2,q}$-norm regularization method to process the collected FMCW SAR data. By considering the ambiguity suppression in the model construction and algorithm implementation, this method can obtain the image with less ambiguities compared to L_q-norm-based method [41].
3) To further speed up the FMCW SAR sparse imaging process, a real-time method based on approximated observation will be reported to make sparse imaging method become an easily used technique for practical FMCW SAR applications [32], [42].
4) In addition, the implementation algorithm of these FMCW SAR sparse imaging methods are unified in this article and their computational complexity will be comprehensively analyzed and compared with MF and conventional observation matrix-based imaging methods, respectively [33].

The rest of this article is organized as follows. In Section II, we will briefly introduce the principle of conventional observation matrix-based FMCW SAR sparse imaging method, highlight the main challenges of this conventional method, and demonstrate the necessity of the research to be reported. Then, Section III will discuss the approximated observation-based imaging technique via L_q-norm regularization recovery. In Section IV, to minimize the azimuth ambiguity, the proposed approximated observation-based $L_{2,q}$-norm regularization method is introduced from 2-D unambiguous imaging model establishment to mixed norm-based regularization recovery scheme. Motivated by the concept of approximated observation, an improved real-time sparse imaging method is demonstrated in Section V. Then, the comprehensive analysis and comparison of these approximated observation sparse imaging methods will be shown in Section VI. Finally, in Section VII, conclusions are drawn to summarize our current work in this direction.

II. Observation Matrix-Based FMCW SAR Sparse Imaging

In the process of FMCW SAR data collection, we assume the surveillance region is rectangular, with N_U pixels in azimuth and N_W pixels in range, and characterize a point by its 2-D index (u, w). Let $\mathbf{X}$ denote a $N_U \times N_W$ matrix whose (u, w) entry is scattering amplitude $x(u, w)$, and $\mathbf{x} = \mathrm{vec}(\mathbf{X}) \in \mathbb{C}^{N \times 1}$ with $N = N_U \times N_W$, where the operation $\mathrm{vec}(\cdot)$ stacks the matrix columns one after the other. Let $\lfloor a \rfloor$ represent the floor of a nonnegative real number a. For $1 \leq n \leq N$, we define $u_n = \lfloor (n-1)/N_U \rfloor + 1$ and $w_n = n - (u_n - 1)N_U$. Then, the nth entry of $\mathbf{x}$ is $x(u_n, w_n)$. Let $s(t_r) = \exp\{j2\pi f_0 t_r + j\pi K_r t_r^2\}$ represent the transmitted signal, where f_0 is the carrier frequency, K_r is the chirp rate, and t_r is the range time. The

dechirp-on-receive signal at time (t_a, t_r) can be expressed as [5]

$$y(t_a,t_r) = \sum_{n=1}^{N} x(u_n,w_n)\cdot\exp\{-j2\pi f_0\tau_d(n)\} \cdot\exp\{-j2\pi K_r\tau_d(n)t_r\}\cdot\exp\{j\pi K_r\tau_d(n)^2\} \quad (1)$$

where t_a is the azimuth time, and $\tau_d(n)$ is the wave propagation round-trip delay time of the nth entry, which is given by

$$\tau_d(n) = \frac{2c^2}{c^2-v^2}\left[\frac{R(t_a,t_r;p_n,q_n)}{c}+\frac{v^2}{c^2}(t_a+t_r-\tau_n)\right] \quad (2)$$

where c is the speed of light, v is the velocity of platform, τ_n is the zero-Doppler time of point $x(u_n, w_n)$, and $R(t_a, t_r; u_n, w_n)$ is the instantaneous slant range at time (t_a, t_r) of the nth point. Let $\mathbf{Y}_f \cong \{y(t_a,t_r)\} \in \mathbb{C}^{N_a\times N_r}$ represent the fully sampled 2-D raw data. Then, the typical MF imaging procedure, $\mathcal{R}(\cdot)$, can be expressed as [33]

$$\mathbf{X}_{\mathrm{MF}} = \mathcal{R}(\mathbf{Y}_f). \quad (3)$$

Several MF-based algorithms, such as RDA [7], FSA [8], WDA [9], and BPA [10], can achieve accurate reconstruction of the surveillance regions via the imaging process in (3), and obtain high-resolution SAR images. However, it is difficult to use these methods to further improve the recovered image quality in terms of sidelobes and noise suppression, as well as recover the sparse scene from down-sampled data.

To solve the above-mentioned problems of MF-based methods, sparse signal processing technique was introduced to FMCW SAR. Let $\mathbf{y}_f = \mathrm{vec}(\mathbf{Y}_f) \in \mathbb{C}^{L\times 1}$ with $L = N_a \times N_r$. By denoting the sampling matrix as $\mathbf{\Psi} \cong \{\psi_m\} \in \mathbb{R}^{M\times L}$, $M \le L$, we can express the 1-D down-sampled raw data $\mathbf{y} \in \mathbb{C}^{M\times 1}$ as

$$\mathbf{y} = \mathbf{\Psi}\mathbf{y}_f = \mathbf{\Psi}\mathbf{A}\mathbf{x} + \mathbf{n}_0 = \mathbf{\Phi}\mathbf{x} + \mathbf{n}_0 \quad (4)$$

where $\mathbf{A} \cong \{A(l,n)\}_{L\times N}$ is the system observation matrix, $\mathbf{\Phi} \cong \{\phi(m,n)\}_{M\times N}$ is the system measurement matrix, and $\mathbf{n}_0$ is the noise vector. If raw data $\mathbf{y}$ is band limited, i.e., down-sampled data, the model in (4) leads to an ill-conditioned inverse problem, which has either no solution or infinitely many solutions. Therefore, some assumptions are needed to obtain the unique solution of (4). As discussed in [16]–[18], if $\mathbf{x}$ is sparse enough, i.e., $\|\mathbf{x}\|_0 \ll L$, and $\mathbf{\Phi}$ satisfies the condition of restricted isometry property, we can recover $\mathbf{x}$ by solving the L_q-norm regularization problem

$$\hat{\mathbf{x}} = \min_{\mathbf{x}}\left\{\|\mathbf{y}-\mathbf{\Phi}\mathbf{x}\|_2^2 + \lambda\|\mathbf{x}\|_q^q\right\} \quad (5)$$

where λ is the regularization parameter. Several algorithms can be used to solve the above optimization problem. When $q = 0$, the iterative hard thresholding algorithm [34] and greedy algorithm [35] can be utilized for the scene recovery. Furthermore, when $\mathbf{x}$ is sparse enough, an L_1-norm can be used to replace the L_0-norm to achieve the regularization reconstruction, known as basis pursuit [36] or least absolute shrinkage and selection operator (Lasso) solution [37]. For example, iterative soft thresholding (IST) algorithm [38] and complex approximated message passing (CAMP) algorithm [39] have been reported in the works of literature to solve the L_1-norm optimization problem. In 2012, the idea of $L_q(0 < q < 1)$-norm regularization was proposed to obtain more sparse solution than L_1-norm [40]. Without loss of generality, we select IST as an example in this article for solving different kinds of L_q-norm regularization problems.

Conventional observation matrix-based sparse imaging method has shown desirable merits in several aspects, such as imaging performance improvement, super-resolving focusing, and sparse scene recovery from down-sampled data. However, it needs too much computational complexity to transfer the 2-D raw data into a vector to achieve the azimuth-range decoupling in sparse reconstruction, which becomes a major obstacle to be applied for practical large-scale scene recovery [23]–[25].

III. Approximated Observation-Based FMCW SAR Sparse Imaging for Large-Scale Scene Recovery

Similar to 1-D imaging, we can write the 2-D FMCW SAR imaging model as

$$\mathbf{Y} = \mathbf{\Xi}_a \circ \mathbf{Y}_f \circ \mathbf{\Xi}_r = \mathbf{\Xi}_a \circ (\mathbf{H}\mathbf{X}) \circ \mathbf{\Xi}_r + \mathbf{N}_0 \quad (6)$$

where the symbols are defined as follows.

Due to the existence of azimuth-range coupling in the 2-D echo data domain, $\mathbf{H}$ could not be constructed directly as $\mathbf{A}$ in (4). Thus it is impossible to achieve sparse reconstruction via the model in (6). An alternative method, introduced in Section II, requires too much computational cost especially for the large-scale scene recovery. To solve this problem, an approximated observation-based method was proposed for focusing FMCW-mode SAR image [23], [26], [32], [33]. With the help of (6), the MF imaging procedure in (3) can be rewritten as

$$\mathbf{X}_{\mathrm{MF}} = \mathcal{R}(\mathbf{Y}_f) = \mathcal{R}(\mathbf{H}\mathbf{X}). \quad (7)$$

Due to the existence of sidelobes, noise, and clutter, $\mathbf{X}_{\mathrm{MF}}$ is always the approximation of $\mathbf{X}$. Therefore, if $\mathcal{R}\mathbf{H} = \mathbf{I}$, then we can use $\mathcal{M} = \mathcal{R}^{-1}$, the inverse of MF imaging procedure, to approximate $\mathbf{H}$, where $\mathcal{M}$ is known as echo simulation operator. Thus, the basic idea of the approximated observation can be generalized as

$$\mathcal{M}(\mathbf{X}) = \mathcal{R}^{-1}(\mathbf{X}) = \mathbf{H}\mathbf{X}. \quad (8)$$

With the above replacement, the 2-D FMCW SAR imaging model can be written as [33]

$$\mathbf{Y} = \mathbf{\Xi}_a \circ \mathbf{Y}_f \circ \mathbf{\Xi}_r = \mathbf{\Xi}_a \circ \mathcal{M}(\mathbf{X}) \circ \mathbf{\Xi}_r + \mathbf{N}_0. \quad (9)$$

For the model in (9), we can recover the scene of interest by solving a 2-D L_q-norm regularization problem

$$\hat{\mathbf{X}} = \min_{\mathbf{X}}\left\{\|\mathbf{Y}-\mathbf{\Xi}_a\circ\mathcal{M}(\mathbf{X})\circ\mathbf{\Xi}_r\|_F^2 + \lambda\|\mathbf{X}\|_q^q\right\}. \quad (10)$$

For clarity, this approximated observation-based sparse imaging method is known as L_q-De. The key of L_q-De is the construction of $\mathcal{M}$, which can be implemented based on existing MF-based imaging algorithms. Fig. 1 shows the three typical MF-based FMCW SAR imaging procedures. The abbreviations in Fig. 1 are defined as follows.

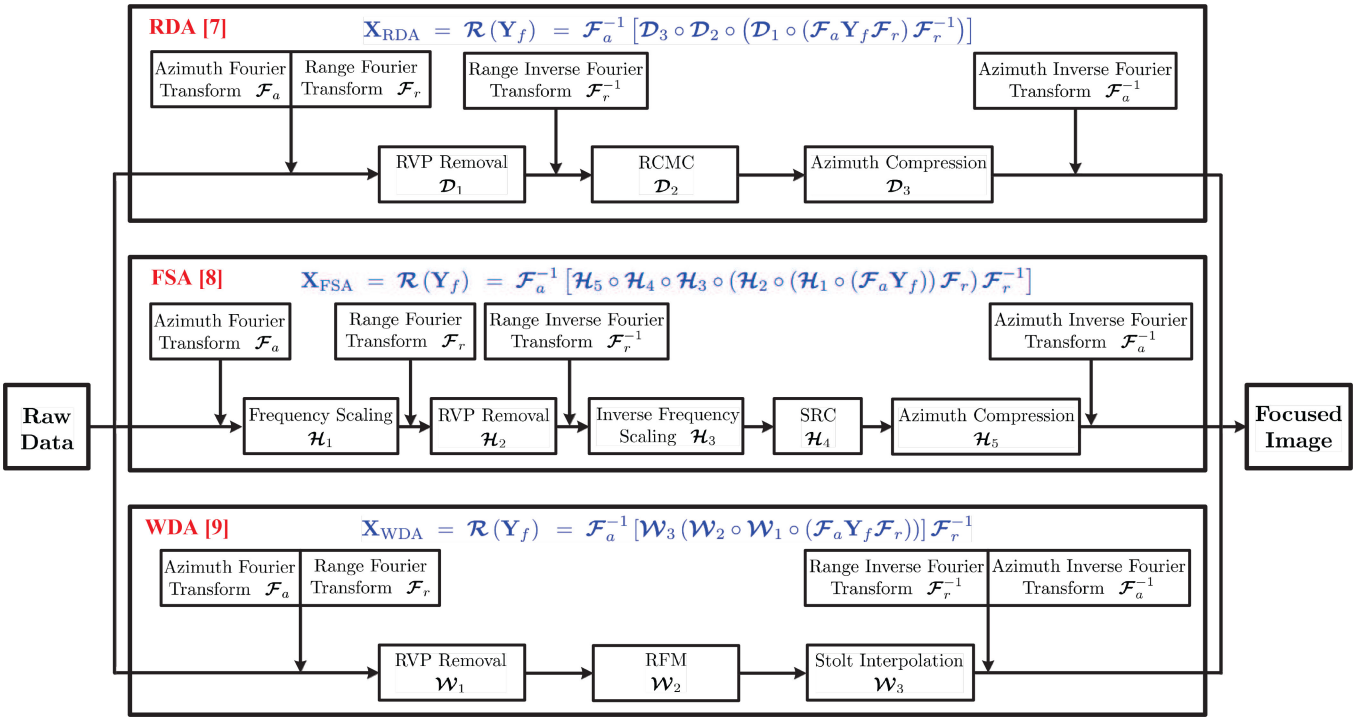

Fig. 1. Flow diagrams of different MF-based methods for FMCW SAR imaging.

It is seen that nearly all steps in these methods, i.e., $\mathcal{D}_1$ and $\mathcal{D}_3$ in RDA [7], $\mathcal{H}_1 - \mathcal{H}_5$ in FSA [8], and $\mathcal{W}_1, \mathcal{W}_2$ in WDA [9], are achieved by Hadamard product indicated by symbol $\circ$. Thus their conjugate matrices, denoted by $(\cdot)^*$, can be used for describing the echo simulation procedure. Only two operations, RCMC $\mathcal{D}_2$ in RDA, and Stolt interpolation processing $\mathcal{W}_3$ in WDA, cannot be achieved by simple phase multiplication. Thus, the required inverse steps, $\mathcal{D}_2^{\dagger}$ and $\mathcal{W}_3^{\dagger}$ in $\mathcal{M}$, are achieved by interpolation operation. According to the above analysis and the imaging procedures in Fig. 1, we can write the detailed expressions as follows.

Constructed $\mathcal{M}$ based on RDA

$$\mathcal{M}(\cdot) = \mathcal{F}_a^{-1}[\mathcal{D}_1^* \circ (\mathcal{D}_2^{\dagger}(\mathcal{D}_3^* \circ (\mathcal{F}_a(\cdot)))\mathcal{F}_r)]\mathcal{F}_r^{-1}. \quad (11a)$$

Constructed $\mathcal{M}$ based on FSA

$$\mathcal{M}(\cdot) = \mathcal{F}_a^{-1}\left[\mathcal{H}_1^* \circ (\mathcal{H}_2^* \circ (\mathcal{H}_3^* \circ \mathcal{H}_4^* \circ \mathcal{H}_5^* \circ (\mathcal{F}_a(\cdot)))\,\mathcal{F}_r)\,\mathcal{F}_r^{-1}\right]. \quad (11b)$$

Constructed $\mathcal{M}$ based on WDA

$$\mathcal{M}(\cdot) = \mathcal{F}_a^{-1}[\mathcal{W}_1^* \circ \mathcal{W}_2^* \circ \mathcal{W}_3^{\dagger}(\mathcal{F}_a(\cdot)\mathcal{F}_r)]\mathcal{F}_r^{-1}. \quad (11c)$$

With help of constructed $\mathcal{M}$ in (11), several algorithms have been proposed to solve the L_q-norm regularization problem in (10), such as IST-based method [26] and CAMP-based method [28]. In L_q-norm regularization-based sparse imaging, theoretically, the smaller the value of q, the more sparse solution will be obtained. In real data processing, however, it is found that there is almost no difference in the reconstructed images for different values of q. Therefore, we usually take $q = 1$ as an example for the real data processing. The flow diagram of iterative recovery algorithm for the model in (10) is shown in Fig. 2. It should be noted that for the model in (10), three different kinds of $\mathcal{M}$ in (11) have a similar effect in algorithm implementation when performing the echo data collection process. Therefore,

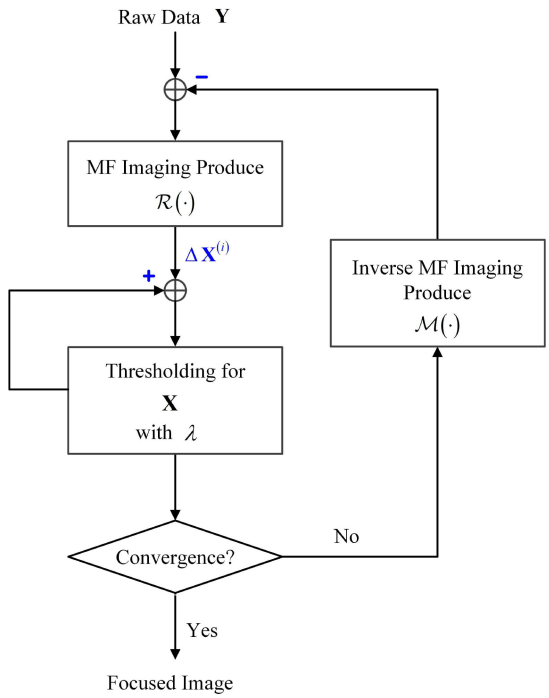

Fig. 2. Flow diagram of iterative recovery algorithm for the model in (10).

for spare imaging based on model in (10), we need to select one of MF-based imaging algorithms to construct operators $\mathcal{R}$ and $\mathcal{M}$, and guarantee the consistency of $\mathcal{R}$ and $\mathcal{M}$ in the process of iterative recovery.

In [32], the analysis of computational cost shows that compared to observation matrix-based sparse imaging method, named as L_q-Ob, L_q-De method reduces the computational complexity by one to two orders of that needed by MF, which makes sparse imaging of large-scale scene in FMCW SAR possible. The detailed analysis and comparison on the computational complexities needed by the different kinds of sparse imaging methods will be performed in Section VI.

IV. Approximated Observation-Based FMCW SAR Sparse Imaging for Ambiguity Suppression

In SAR imaging, due to the finite azimuth sampling frequency, i.e., PRF, frequencies outside $[f_{\text{dc}} - \text{PRF}/2, f_{\text{dc}} + \text{PRF}/2]$ will be folded into the main Doppler spectrum band, which causes the azimuth ambiguity [3], where f_{dc} is the Doppler center frequency. The center frequency of the ith azimuth ambiguity in the Doppler spectrum domain is

$$f_c = f_{\text{dc}} + i \cdot \text{PRF}, \quad i \in \mathbb{Z} \quad \text{and} \quad i \neq 0 \tag{12}$$

where $i \in \mathbb{Z}^-$ and $i \in \mathbb{Z}^+$ are the shifting indexes of ambiguity Doppler spectrum in the left and right sides of the main spectrum ($i = 0$), respectively. The above-mentioned relationship between original target and its azimuth ambiguities can be regarded as a group-sparsity property, which can be solved by using the regularization-based method [23].

Let $\mathcal{R}_i$ and $\mathcal{M}_i$ denote the MF and inverse imaging procedures of ith azimuth ambiguity, $i \in \mathbb{Z}$ and $\mathcal{R}_0 = \mathcal{R}$, $\mathcal{M}_0 = \mathcal{M}$. It is easy to know that $\mathcal{R}_i$ has the same expression as $\mathcal{R}$, only with different azimuth frequency f_a used in the imaging process. $\mathcal{M}_i$ can be also obtained in the same way. Then, we can rewrite the 2-D sparse SAR imaging model in (9) as

$$\mathbf{Y} = \mathbf{\Xi}_a \circ \mathbf{Y}_f \circ \mathbf{\Xi}_r = \mathbf{\Xi}_a \circ \sum_i \mathcal{M}_i(\mathbf{X}_i) \circ \mathbf{\Xi}_r + \mathbf{N}_0 \tag{13}$$

and obtain the unambiguous sparse image as

$$\hat{\mathbf{X}} = \min_{\mathbf{X}} \left\{ \left\| \mathbf{Y} - \mathbf{\Xi}_a \circ \sum_i \mathcal{M}_i(\mathbf{X}_i) \circ \mathbf{\Xi}_r \right\|_F^2 + \lambda_1 \left\| \sum_i \mathbf{X}_i \right\|_{2,q}^q + \lambda_2 \|\mathbf{X}\|_q^q \right\}, q \in (0, 1] \tag{14}$$

with

$$\left\| \sum_i \mathbf{X}_i \right\|_{2,q}^q = \left[\sum_u \left(\sum_w \left| \sum_i \mathbf{X}_i(u, w) \right|^2 \right)^{q/2} \right]^{1/q} \tag{15}$$

where $\mathbf{X}_0 = \mathbf{X}$, and $\mathbf{X}_i \in \mathbb{C}^{N_U \times N_W}$ is the backscattering coefficient of the ith azimuth ambiguity. In (14), the $L_{2,q}$-norm term represents the group sparsity penalty of $\mathbf{X}_i$ with regularization parameter λ_1, and the L_q-norm term restricts the scene sparsity penalty with λ_2. The flow diagram of iterative recovery algorithm for the model in (14) is shown in Fig. 3. For clarity, this ambiguity suppression method is named as $L_{p,q}$-De. When $q = 1$, the detailed iterative recovery procedures are listed in [41].

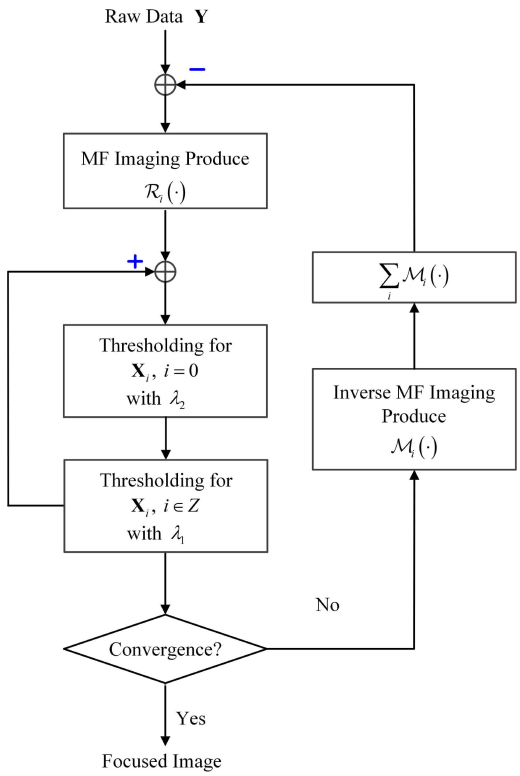

Fig. 3. Flow diagram of iterative recovery algorithm for the model in (14).

Let us explain how $L_{2,q}$-De achieves the effective suppression of azimuth ambiguity in FMCW SAR sparse imaging. We first consider the azimuth ambiguity terms in the constructed model in (13). After exploiting the group sparsity of ambiguity and original imaging targets, the proposed method shown in Fig. 3 can effectively suppress the ambiguity through $L_{2,q}$-norm regularization operation in iterative recovery, and hence obtain the high-resolution unambiguous image.

V. Complex Image-Based FMCW SAR Real-Time Sparse Imaging

In order to further reduce the computational complexity of sparse imaging for real-time data processing, a complex image-based FMCW SAR sparse imaging method was proposed and successfully used in imaging performance improvement [42]. For the collected full-sampling echo data $\mathbf{Y}_f$, similar to (9), we can express the relationship between $\mathbf{Y}_f$ and $\mathbf{X}$ as

$$\mathbf{Y}_f = \mathcal{M}(\mathbf{X}) + \mathbf{N}_0. \tag{16}$$

Then, performing the MF operation $\mathcal{R}(\cdot)$ on both sides of (16), we have

$$\begin{aligned} &\mathcal{R}(\mathbf{Y}_f) = \mathcal{R}(\mathcal{M}(\mathbf{X})) + \mathcal{R}(\mathbf{N}_0) \\ &\Leftrightarrow \mathbf{X}_{\text{MF}} = \mathbf{X} + \mathbf{N} \end{aligned} \tag{17}$$

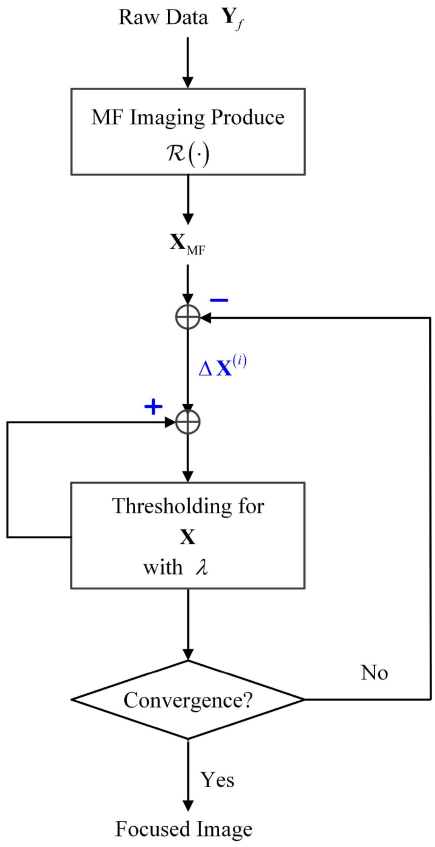

Fig. 4. Flow diagram of iterative recovery algorithm for the model in (18).

where $\mathbf{N} = \mathcal{R}(\mathbf{N}_0) \in \mathbb{C}^{N_U \times N_W}$ is a matrix that denotes the difference between $\mathbf{X}_{\mathrm{MF}}$ and $\mathbf{X}$ to include all kinds of artifacts such as noise and sidelobes. Then, the scene $\mathbf{X}$ can be recovered by solving the 2-D L_q-norm regularization problem

$$\hat{\mathbf{X}} = \min_{\mathbf{X}} \left\{ \|\mathbf{X}_{\mathrm{MF}} - \mathbf{X}\|_F^2 + \lambda \|\mathbf{X}\|_q^q \right\}. \tag{18}$$

The flow diagram of the iterative recovery algorithm for the model in (18) can be summarized in Fig. 4. As discussed in [42], when the data are fully sampled, the method in Fig. 4, named as L_q-Re, can achieve identical sparse imaging result to that of L_q-De in Section III. It is important to be aware that this method effectively reduces the computational complexity of sparse imaging to be infinitely close to that needed by MF-based method, which enables the real-time data processing. In addition, in the absence of original echo data, L_q-Re can still be processed-based on the MF recovered complex image to improve the image quality. Of course, it also has an undesirable limitation of processing the down-sampled echo data that may be required by some applications.

VI. Comparison of Approximated Observation-Based FMCW SAR Sparse Imaging Methods

A. Computational Complexity and Memory Requirement

Compared to observation matrix-based sparse imaging method, the main superiority of approximated observation-based methods is the reduced requirements of computation and data memory, which allows it to process the large-scale scenes. Let $M = N_a \times N_r$ and $N = N_U \times N_W$ represent the number of points in the echo data $\mathbf{Y}$ and considered scene $\mathbf{X}$, I_1 denotes the required steps of the iterative recovery algorithms for L_q-Ob described in (5) [23], L_q-De in (10) [26], $L_{2,q}$-De in (14) [41], and L_q-Re in (18) [42]. Because these algorithms [23], [26], [41], [42] use the similar iterative recovery principle, they need similar steps for the algorithm convergence. In practical SAR data, because only the first left and right ambiguity areas can be seen in the focused image, we normally set $I = 3$ in $L_{2,q}$-De to include the main imaging area, the first left and the first right ambiguity areas.

In Table I, we have listed the computational complexities needed by MF, conventional observation-based, and approximated observation-based FMCW SAR sparse imaging methods, respectively. It is found that influenced by the vectorization operation of echo data and considered scene, the computational complexity of L_q-Ob has reached a squared order of scene size, i.e., $\mathcal{O}(I_1 MN)$, which is unacceptable for the large-scale scene recovery. In contrast, the approximated observation-based sparse imaging methods have reduced the complexity close to that of MF with $\mathcal{O}(M \log(M))$. In addition, it can be seen that compared with MF-based method, the complexity of L_q-Re is increased only by the thresholding process $\mathcal{O}(I_1\ N)$, which is the main reason of L_q-Re can be used for real-time sparse imaging. Table I also lists the memory requirement of discussed methods. It is seen that all approximated observation-based methods reduce the memory size to the same order as that of MF, which is far below the requirement of L_q-Ob. This means that the memory capacity of the computing platform is no longer the obstacle of sparse imaging.

B. Sparse Imaging From Fully Sampled Data

When the data are fully sampled, as listed in Table I, it is seen that all the sparse imaging methods can be applied for the sparse and nonsparse scene recovery. In this case, these sparse imaging methods can be simply regarded as the regularization-based SAR imaging approach, because the requirements of the sampling theorem are met. Figs. 5 and 6 show the recovered images of sparse and nonsparse scenes by MF, L_q-De, $L_{2,q}$-De, and L_q-Re from full-sampled echo data. Experimental parameters of all simulated and real data-based experiments are shown in Table II. Consistent with the theoretical analysis in Table I, it is seen that all sparse imaging methods can well reconstruct the considered scene, regardless of whether the scene is sparse or not. Compared with the typical MF-based result, it is found that the focused image of the sparse imaging methods have better performance, such as less noise, clutter and sidelobes, especially in the area with weak backscattering amplitude. It should be noted that in all experiments reported in this article, we use FSA as the example to construct operators $\mathcal{R}$ and $\mathcal{M}$ to validate the approximated observation-based sparse imaging methods.

C. Sparse Imaging From Down-Sampled Data

When the collected data no longer satisfy the requirement of sampling theorem, as shown in Figs. 7(e) and (i) and 8(b), MF method could not recover the simulated scene any more.

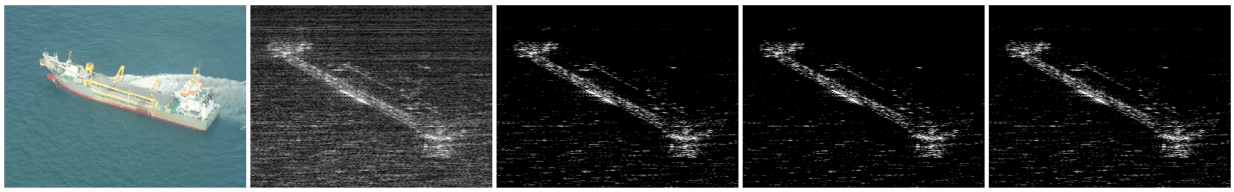

(a) (b) (c) (d) (e)

Fig. 5. (a) Optical image of ship target. Recovered images of sparse scene by (b) MF, (c) L_q-De, (d) $L_{2,q}$-De, and (e) L_q-Re, respectively. The input data are fully sampled. Horizontal axis is the azimuth direction.

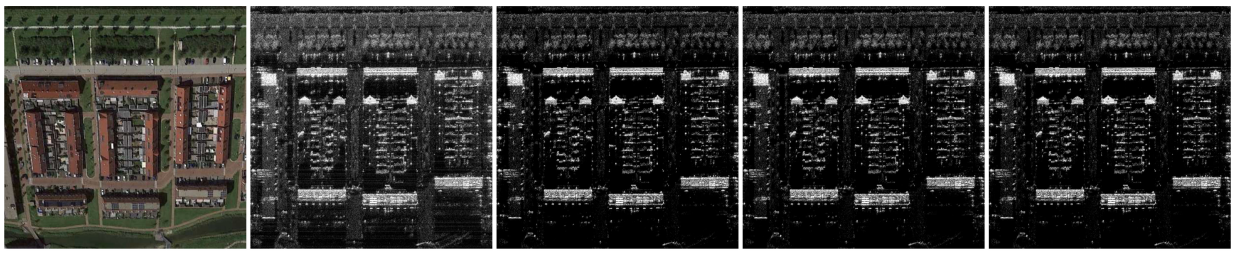

(a) (b) (c) (d) (e)

Fig. 6. (a) Optical image of surveillance region (Google Earth). Recovered images of nonsparse scene by (b) MF, (c) L_q-De, (d) $L_{2,q}$-De, and (e) L_q-Re, respectively. The input data are fully sampled. Horizontal axis is the azimuth direction.

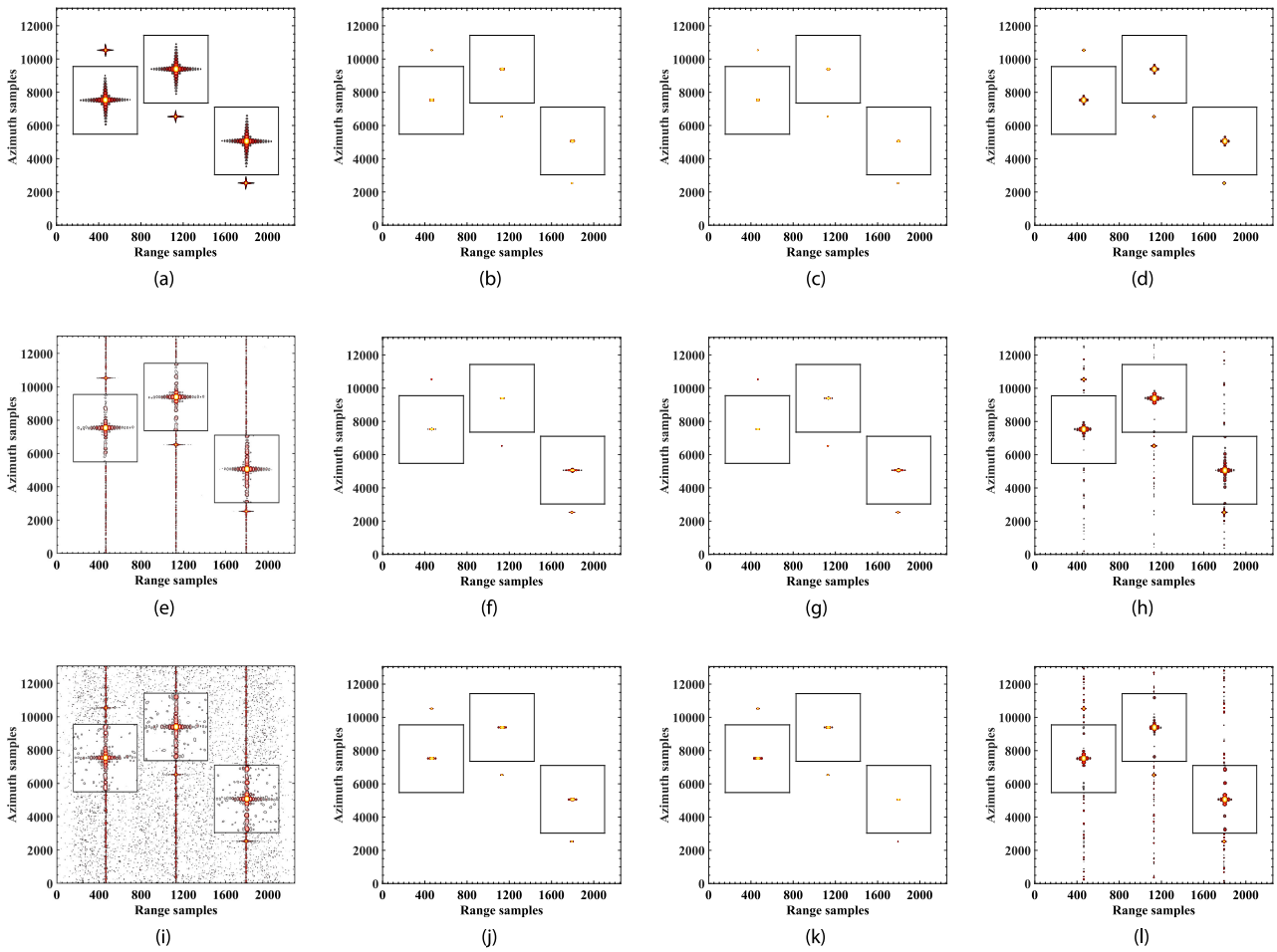

Fig. 7. Recovered images of sparse simulated scene from down-sampled data by (from left to right column) MF, L_q-De, $L_{2,q}$-De, and L_q-Re, respectively. The sampling ratios are 100%, 20%, and 10% from upper to lower row, respectively.

TABLE I
COMPARISON OF DIFFERENT FMCW SAR SPARSE IMAGING METHODS

Algorithm	Regularization Recovery Model	Computational Complexity
MF	$\mathbf{X}_{\mathrm{MF}} = \mathcal{R}(\mathbf{Y}_f)$	$\mathcal{O}(M \log M)$
L_q-Ob	$\hat{\mathbf{x}} = \min_{\mathbf{x}} \left\{ \|\mathbf{y} - \mathbf{\Phi}\mathbf{x}\|_2^2 + \lambda \|\mathbf{x}\|_q^q \right\}$	$\mathcal{O}(I_1 MN)$
L_q-De	$\hat{\mathbf{X}} = \min_{\mathbf{X}} \left\{ \|\mathbf{Y} - \mathbf{\Xi}_a \circ \mathcal{M}(\mathbf{X}) \circ \mathbf{\Xi}_r\|_F^2 + \lambda \|\mathbf{X}\|_q^q \right\}$	$\mathcal{O}(I_1 (M \log(M) + N))$
$L_{2,q}$-De	$\hat{\mathbf{X}} = \min_{\mathbf{X}} \left\{ \left\| \mathbf{Y} - \mathbf{\Xi}_a \circ \sum_i \mathcal{M}_i(\mathbf{X}_i) \circ \mathbf{\Xi}_r \right\|_F^2 + \lambda_1 \left\| \sum_i \mathbf{X}_i \right\|_{2,q}^q + \lambda_2 \|\mathbf{X}\|_q^q \right\}$	$\mathcal{O}(I_1 (IM \log(M) + 2N))$
L_q-Re	$\hat{\mathbf{X}} = \min_{\mathbf{X}} \left\{ \|\mathbf{X}_{\mathrm{MF}} - \mathbf{X}\|_F^2 + \lambda \|\mathbf{X}\|_q^q \right\}$	$\mathcal{O}(M \log(M) + I_1 N)$

Algorithm	Memory Need	Full-sampled Data	Down-sampled Data	Large Scene Imaging	Real-time Imaging
MF	$\mathcal{O}(N)$	All scenes	Failed	Yes	Yes
L_q-Ob	$\mathcal{O}(MN)$	All scenes	Sparse Scene	No	No
L_q-De	$\mathcal{O}(N)$	All scenes	Sparse Scene	Yes	No
$L_{2,q}$-De	$\mathcal{O}(N)$	All scenes	Sparse Scene	Yes	No
L_q-Re	$\mathcal{O}(N)$	All scenes	Failed	Yes	Yes

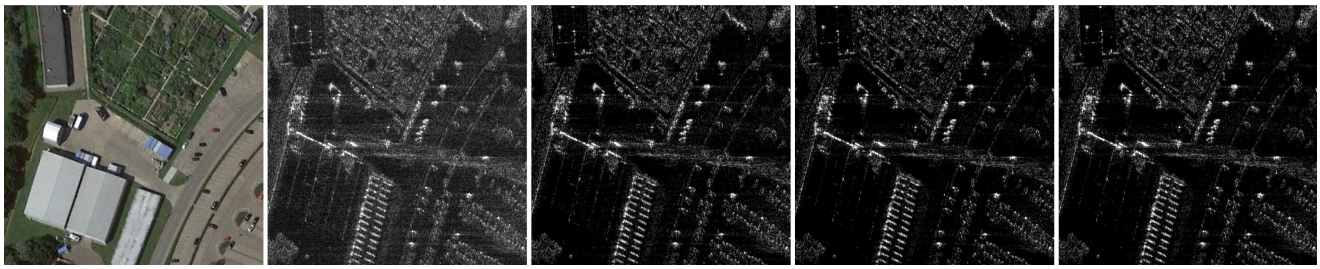

Fig. 8. (a) Optical image of surveillance region (Google Earth). Recovered images of nonsparse scene from 80% down-sampled data by (b) MF, (c) L_q-De, (d) $L_{2,q}$-De, and (e) L_q-Re, respectively. Horizontal axis is the azimuth direction.

TABLE II
EXPERIMENTAL PARAMETERS

Parameter	Value
Velocity of platform	$\approx$ 60 m/s
Radar center frequency	9.6 GHz
Pulse repetition frequency	2894.86 Hz
Bandwidth	600 MHz
Platform height	3000 ft
Range sampling rate	50 MHz

Its reconstructed images have obvious energy dispersion along the azimuth direction, especially for the targets with strong backscattering. Since L_q-Re is the regularization operation on the basis of MF recovered images, it cannot remedy the defocused image due to the lack of data. Thus, L_q-Re either cannot obtain the well focused image from down-sampled data [42] [see Figs. 7(h) and (l) and 8(e)].

For the sparse scene, L_q-De and $L_{2,q}$-De can achieve high-resolution sparse images from down-sampled data even with a sampling ratio of 10%. This is in accordance with the theoretical analysis, that is, the approximated observation-based FMCW SAR sparse imaging methods have the down-sampling imaging capability that is similar to the observation matrix-based imaging method. However, the main advantage is to efficiently process the data for large-scale images. In addition, Fig. 7 also shows that compared with MF, the sparse imaging methods can suppress sidelobes to make imaging performance improvement. However, when the scene of interest is nonsparse, as shown in Fig. 8, L_q-De and $L_{2,q}$-De are also powerless especially for the strong targets.

D. Azimuth Ambiguity Suppression

To validate the effectiveness of $L_{2,q}$-De in azimuth ambiguity suppression, five point targets with amplitude values of 0.3, 0.5, 1.0, 0.8, 0.3 (from top to bottom) are placed in the surveillance region to simulate the sparse scene. The reason for setting the amplitude values in this way is to ensure that the azimuth ambiguity's amplitude of the strongest target is greater than that of the weakest one. Fig. 9 depicts the recovered images

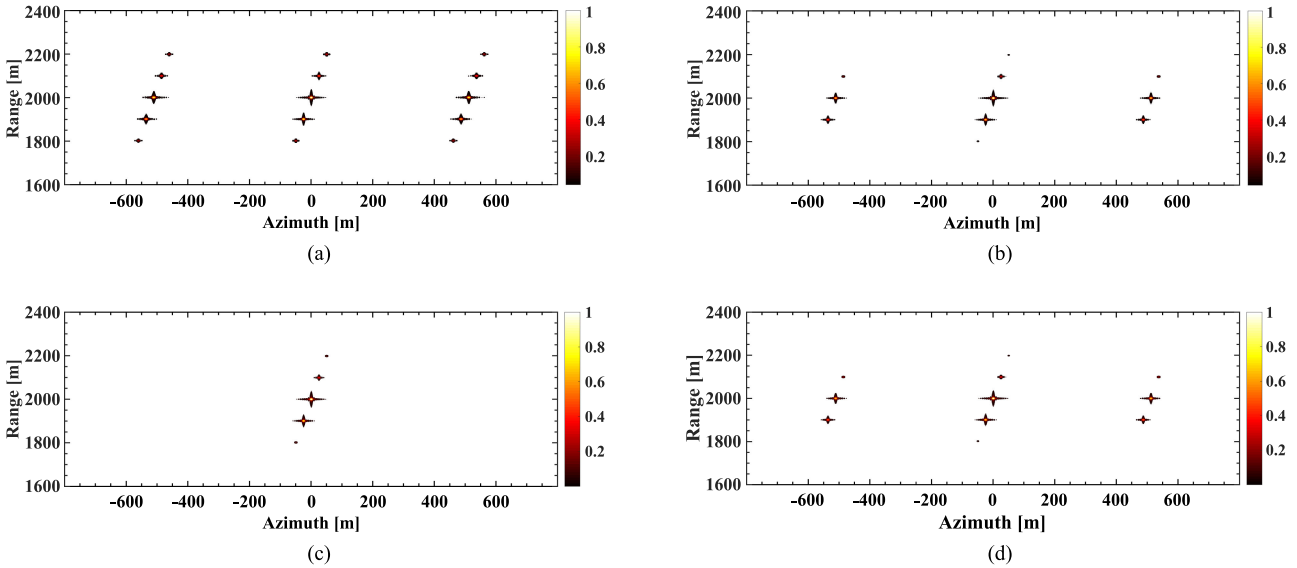

Fig. 9. Recovered images of sparse scene by (a) MF, (b) L_q-De, (c) $L_{2,q}$-De, and (d) L_q-Re, respectively. The input data are 50% uniform down-sampled.

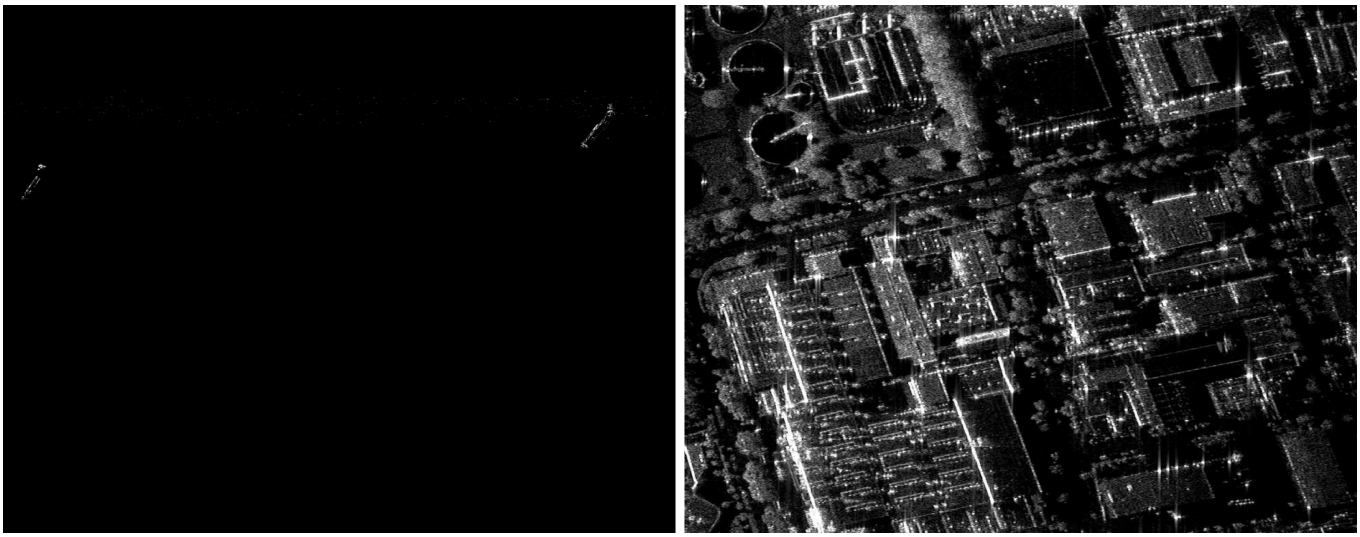

Fig. 10. Recovered images of (a) sparse scene by L_q-De from 30% random down-sampled data and (b) nonsparse scene by L_q-De from fully sampled data.

by MF, L_q-De, $L_{2,q}$-De, and L_q-Re, respectively, from 50% uniform down-sampled data. It can be seen that due to the lack of data, the image recovered by the MF method shows obvious ambiguity in the azimuth direction, and hence results in the failed reconstruction. L_q-De can suppress ambiguity of weak targets based on the regularization constraints and cannot do much reduction of strong ambiguity. The main reason is that the ambiguities' amplitude of the targets with strong backscattering are stronger than the weak targets, which makes these ambiguities being recovered as the targets. After constructing the ambiguity term into the imaging model and suppressing it during the iterative process, $L_{2,q}$-De effectively solves the problem of azimuth ambiguity suppression, and achieves the accurate recovery of considered scene.

E. Sparse Imaging for Large-Scale Scene

In terms of computational cost reduction, the proposed sparse imaging method based on approximated observation is used for the practical large-scene FMCW SAR data. Using L_q-De as example, we reconstruct the sparse ocean surface with a size of 80000×3000 (Azimuth $\times$ Range) and nonsparse city area with a size of 20000×1500 (Azimuth $\times$ Range) from 30% random down-sampled and fully sampled data, respectively. Similar to

the above experimental results, Fig. 10 shows that L_q-De can recover the large-scale sparse scene from down-sampled data and nonsparse area from fully sampled data with reduced noise and clutter.

VII. Conclusion

In this article, we have presented an overview of our recent research on FMCW SAR sparse imaging algorithms based on approximated observation. Facing the challenges of high-resolution, wide-swath, and real-time processing in modern SAR system, we have illustrated a solution based on the sparse signal processing technology. For the sparse scene observation, we can decrease the PRF in data collection, equivalent to azimuth down-sampling, to reduce the system complexity and improve the swath width. The sparse imaging method for large-scale scene discussed in this article is particularly suitable to obtain high-resolution FMCW SAR image from the down-sampled data. For both sparse and nonsparse surveillance regions, we can use the existing FMCW SAR radar system for the data collection without any changes, exploit the approximated observation-based method for image focusing, and utilize the discussed sparse imaging method for high-resolution large-scale scene reconstruction in real-time. In addition, to suppress azimuth ambiguities, a novel approximated observation-based $L_{2,q}$-norm regularization method is proposed to obtain the image with less ambiguities compared to L_q-norm-based method. Because sparse signal processing techniques have shown to achieve excellent performance and promising potentials in FMCW SAR imaging, we have already used it frequently to process practical data to achieve large-scale high-resolution images.

References

[1] J. C. Curlander and R. N. Mcdonough, *Synthetic Aperture Radar: System and Signal Processing*. New York, NY, USA: Wiley, 1991.

[2] F. M. Henderson and A. J. Lewis, *Principle and Application of Imaging Radar*. New York, NY, USA: Wiley, 1998.

[3] I. G. Cumming and F. H. Wong, *Digital Processing of Synthetic Aperture Radar Data: Algorithms and Implementation*. Norwood, MA, USA: Artech House, 2004.

[4] A. G. Stove, "Linear FMCW radar techniques," *Inst. Elect. Eng. Proc. F—Radar Signal Process.*, vol. 139, no. 5, pp. 343–350, 1992.

[5] A. Meta, P. Hoogeboom, and L. P. Ligthart, "Signal processing for FMCW SAR," *IEEE Trans. Geosci. Remote Sens.*, vol. 45, no. 11, pp. 3519–3532, Nov. 2007.

[6] Z. Jiang, H. Kan, and J. Wan, "A chirp transform algorithm for processing squint mode FMCW SAR data," *IEEE Trans. Geosci. Remote Sens. Lett.*, vol. 4, no. 3, pp. 377–381, Jul. 2007.

[7] J. J. M. de Wit, A. Meta, and P. Hoogeboom, "Modified range-Doppler processing for FM-CW synthetic aperture radar," *IEEE Geosci. Remote Sens. Lett.*, vol. 3, no. 1, pp. 83–87, Jan. 2006.

[8] A. Meta, P. Hoogeboom, and L. P. Ligthart, "Non-linear frequency scaling algorithm for FMCW SAR data," in *Proc. 3rd Eur. Radar Conf.*, Manchester, U.K., 2006, pp. 9–12.

[9] R. Wang, O. Loffeld, H. Nies, S. Knedlik, M. Hägelen, and H. Essen, "Focus FMCW SAR data using the wavenumber domain algorithm," *IEEE Trans. Geosci. Remote Sens.*, vol. 48, no. 4, pp. 2109–2118, Apr. 2010.

[10] A. Ribalta, "Time-domain reconstruction algorithms for FMCW-SAR," *IEEE Geosci. Remote Sens. Lett.*, vol. 8, no. 3, pp. 396–400, May 2011.

[11] Y. Liu, Y. Deng, and R. Wang, "Focus squint FMCW SAR data using inverse chirp-Z transform based on an analytical point target reference spectrum," *IEEE Geosci. Remote Sens. Lett.*, vol. 9, no. 9, pp. 866–870, Sep. 2012.

[12] H. Nyquist, "Certain topics in telegraph transmission theory," *Trans. Amer. Inst. Elect. Eng.*, vol. 47, no. 2, pp. 617–644, Jul. 1928.

[13] C. E. Shannon, "Communication in the presence of noise," *Proc. IRE*, vol. 37, no. 1, pp. 10–21, 1949.

[14] P. M. Woodward, *Probability and Information Theory: With Applications to Radar*. New York, NY, USA: Pergamon, 1953.

[15] H. Bi, G. Bi, B. Zhang, W. Hong, and Y. Wu, "From theory to application: Real-time sparse SAR imaging," *IEEE Trans. Geosci. Remote Sens.*, vol. 58, no. 4, pp. 2928–2936, Apr. 2020.

[16] D. L. Donoho, "Compressed sensing," *IEEE Trans. Inf. Theory*, vol. 52, no. 4, pp. 1289–1306, Apr. 2006.

[17] E. T. Candés, and T. Tao, "Near-optimal signal recovery from random projections: Universal encoding strategies," *IEEE Trans. Inf. Theory*, vol. 52, no. 12, pp. 5406–5425, Dec. 2006.

[18] E. T. Candés, J. Romberg, and T. Tao, "Stable signal recovery from incomplete and inaccurate measurements," *Commun. Pure Appl. Math.*, vol. 59, no. 8, pp. 1207–1223, 2006.

[19] M. Çetin and W. C. Karl, "Feature-enhanced synthetic aperture radar image formation based on nonquadratic regularization," *IEEE Trans. Image Process.*, vol. 10, no. 4, pp. 623–631, Apr. 2001.

[20] S. Bhattacharya, T. Blumensath, B. Mulgrew, and M. Davies, "Fast encoding of synthetic aperture radar raw data using compressed sensing," in *Proc. IEEE/SP 14th Workshop Statist. Signal Process.*, 2007, pp. 448–452.

[21] M. T. Alonso, P. L. Dekker, and J. Mallorqui, "A novel strategy for radar imaging based on compressive sensing," *IEEE Trans. Geosci. Remote Sens.*, vol. 48, no. 12, pp. 4285–4295, Dec. 2010.

[22] V. M. Patel, G. R. Easley, D. M. Healy, and R. Chellappa, "Compressed synthetic aperture radar," *IEEE J. Sel. Topics Signal Process.*, vol. 4, no. 2, pp. 244–254, Apr. 2010.

[23] B. Zhang, W. Hong, and Y. Wu, "Sparse microwave imaging: Principles and applications," *Sci. China Inf. Sci.*, vol. 55, no. 8, pp. 1–33, 2012.

[24] M. Çetin *et al.*, "Sparsity-driven synthetic aperture radar imaging: Reconstruction, autofocusing, moving targets, and compressed sensing," *IEEE Signal Process. Mag.*, vol. 31, no. 4, pp. 27–40, Jul. 2014.

[25] J. Ender, "A brief review of compressive sensing applied to radar," in *Proc. 14th Int. Radar Symp.*, Dresden, Germany, 2013, pp. 1–14.

[26] J. Fang, Z. Xu, B. Zhang, W. Hong, and Y. Wu, "Fast compressed sensing SAR imaging based on approximated observation," *IEEE J. Sel. Topics Appl. Earth Observ. Remote Sens.*, vol. 7, no. 1, pp. 352–363, Jan. 2014.

[27] X. Dong and Y. Zhang, "A novel compressive sensing algorithm for SAR imaging," *IEEE J. Sel. Topics Appl. Earth Observ. Remote Sens.*, vol. 7, no. 2, pp. 708–720, Feb. 2014.

[28] H. Bi, B. Zhang, X. X. Zhu and W. Hong, "Azimuth-range decouple-based L_1 regularization method for wide ScanSAR imaging via extended chirp scaling," *J. Appl. Remote Sens.*, vol. 11, no. 1, 2017, Art. no. 015007.

[29] H. Bi, B. Zhang, X. X. Zhu, C. Jiang, and W. Hong, "Extended chirp scaling-baseband azimuth scaling-based azimuth-range decouple L_1 regularization for TOPS SAR imaging via CAMP," *IEEE Trans. Geosci. Remote Sens.*, vol. 55, no. 7, pp. 3748–3763, Jul. 2017.

[30] Z. Xu, Z. Wei, C. Wu, and B. Zhang, "Multichannel sliding spotlight SAR imaging based on sparse signal processing," in *Proc. IEEE Inter. Geosci. Remote Sens. Symp.*, Valencia, Spain, 2018, pp. 3703–3706.

[31] B. Zhang, Z. Zhang, C. Jiang, W. Hong, and Y. Wu, "System design and first airborne experiment of sparse microwave imaging radar: Initial results," *Sci. China Inf. Sci.*, vol. 58, no. 6, 2015, Art. no. 062306.

[32] H. Bi, B. Zhang, X. X. Zhu, J. Sun, W. Hong, and Y. Wu, "L_1-regularization-based SAR imaging and CFAR detection via complex approximated message passing," *IEEE Trans. Geosci. Remote Sens.*, vol. 55, no. 6, pp. 3426–3440, Jun. 2017.

[33] H. Bi, J. Wang, and G. Bi, "Wavenumber domain algorithm-based FMCW SAR sparse imaging," *IEEE Trans. Geosci. Remote Sens.*, vol. 57, no. 10, pp. 7466–7475, Oct. 2019.

[34] T. Blumensath and M. E. Davies, "Iterative hard thresholding for compressed sensing," *Appl. Comput. Harmon. Anal.*, vol. 27, no. 3, pp. 265–274, 2009.

[35] S. Mallat and Z. Zhang, "Matching pursuits with time-frequency dictionaries," *IEEE Trans. Signal Process.*, vol. 41, no. 12, pp. 3397–3415, Dec. 1993.

[36] S. S. Chen, D. L. Donoho, and M. A. Saunders, "Atomic decomposition by basis pursuit," *SIAM Rev.*, vol. 43, no. 1, pp. 129–159, 2001.

[37] R. Tibshirani, "Regression shrinkage and selection via the lasso," *J. Roy. Statist. Soc., B (Methodol.)*, vol. 58, no. 1, pp. 267–288, 1996.

[38] I. Daubechies, M. Defriese, and C. De Mol, "An iterative thresholding algorithm for linear inverse problems with a sparsity constraint," *Commun. Pure Appl. Math.*, vol. LVII, pp. 1413–1457, 2004.

[39] A. Maleki, L. Anitori, Z. Yang, and R. Baraniuk, "Asymptotic analysis of complex LASSO via complex approximate message passing (CAMP)," *IEEE Trans. Inf. Theory*, vol. 59, no. 7, pp. 4290–4308, Jul. 2013.
[40] Z. Xu, X. Chang, F. Xu, and H. Zhang, "$L_{1/2}$ regularization: A thresholding representation theory and a fast solver," *IEEE Trans. Neural Netw. Learn Syst.*, vol. 23, no. 7, pp. 1013–1027, Jul. 2012.
[41] H. Bi, D. Zhu, and G. Bi, "$L_{2,1}$-norm regularization based sparse SAR imaging from azimuth periodically sampling data: Initial result," in *Proc. Int. Radar Symp.*, Vilnius, Lithuania, 2020, pp. 1–5.
[42] H. Bi, G. Bi, B. Zhang, and W. Hong, "Complex-image-based sparse SAR imaging and its equivalence," *IEEE Trans. Geosci. Remote Sens.*, vol. 56, no. 9, pp. 5006–5014, Sep. 2018.
[43] H. Bi, G. Bi, B. Zhang, and W. Hong, "A novel iterative thresholding algorithm for complex image based sparse SAR imaging," in *Proc. Eur. Conf. Synthetic Aperture Radar*, Aachen, Germany, 2018, pp. 1453–1457.

Hui Bi (Member, IEEE) was born in Shandong, China, in 1991. He received the bachelor's degree in electronics and information engineering from Yantai University, Yantai, China, in 2012, and the Ph.D. degree in signal and information processing from the University of Chinese Academy of Sciences, Beijing, China, in 2017.

From 2012 to 2017, he was with the Science and Technology on Microwave Imaging Laboratory, Institute of Electronics, Chinese Academy of Sciences, Beijing, China. He was a Research Fellow with the School of Electrical and Electronic Engineering, Nanyang Technological University, Singapore, from 2017 to 2018. Since 2018, he has been with the College of Electronic and Information Engineering, Nanjing University of Aeronautics and Astronautics, Nanjing, China, as an Associate Professor. His research interests include sparse microwave imaging with compressive sensing, synthetic aperture radar data processing and application, sparse signal processing, and tomographic SAR imaging.

Daiyin Zhu was born in Wuxi, China, in 1974. He received the B.S. degree in electronic engineering from the Southeast University, Nanjing, China, in 1996, and the M.S. and Ph.D. degrees in electronics from Nanjing University of Aeronautics and Astronautics (NUAA), Nanjing, China, in 1998 and 2002, respectively.

From 1998 to 1999, he was a Guest Scientist with the Institute of Radio Frequency Technology, German Aerospace Center (DLR), Oberpfaffenhofen, Germany. In 1998, he joined the Department of Electronic Engineering, NUAA, where he is currently a Professor. His research interests include radar imaging algorithms, SAR ground moving target indication, SAR/ISAR autofocus techniques, and SAR interferometry.

Guoan Bi received the B.Sc. degree in radio communications from Dalian University of Technology, Dalian, China, in 1982, and the M.Sc. degree in telecommunication systems and Ph.D. degree in electronics systems from Essex University, Colchester, U.K., in 1985 and 1988, respectively.

Since 1991, he has been with the School of Electrical and Electronic Engineering, Nanyang Technological University, Singapore. His research interests include DSP algorithms and hardware structures, and signal processing for various applications, including sonar, radar, and communications.

Bingchen Zhang was born in 1973. He received the bachelor's degree in electronic engineering and information science from the University of Science and Technology of China, Hefei, China, in 1996, and the master's and Ph.D. degrees from the Institute of Electronics, Chinese Academy of Sciences (IECAS), Beijing, China, in 1999 and 2017, respectively.

Since 1999, he has been with the IECAS, where he is currently a Professor. His research interests include sparse microwave imaging, synthetic aperture radar, radar signal processing, and radar system.

Wen Hong (Senior Member, IEEE) was born in 1968. She received the Ph.D. degree from Beihang University, Beijing, China, in 1997.

She was with the Department of Electrical Engineering, Beihang University, as a faculty member in signal and information processing from 1997 to 2002. In between, she was with the DLR-HF, Wessling, Germany, as a Guest Scientist from 1998 to 1999. Since 2002, she has been with the Institute of Electronics, Chinese Academy of Sciences, Beijing, China, where she is currently a Professor. Her research interests include polarimetric/polarimetric interferometric synthetic aperture radar data processing and application, 3-D SAR signal processing, circular SAR signal processing, and sparse microwave imaging with compressed sensing.

Yirong Wu received the Ms.D. degree from the Beijing Institute of Technology, Beijing, China, in 1988 and the Ph.D. degree from the Institute of Electronics, Chinese Academy of Sciences (IECAS), Beijing, China, in 2001.

Since 1988, he has been with IECAS, where he is currently the Director. He has more than 30 years of experience in remote sensing processing system design. His research interests include microwave imaging, signal and information procession, and related applications.